Dalton Transactions

Cite this: *Dalton Trans.*, 2011, **40**, 7153

www.rsc.org/dalton

PAPER

Fine tuning of emission color of iridium(III) complexes from yellow to red *via* substituent effect on 2-phenylbenzothiazole ligands: synthesis, photophysical, electrochemical and DFT study†

Ming Li,[a] Hui Zeng,[a] Yanyan Meng,[a] Huiqin Sun,[b] Song Liu,[a] Zhiyun Lu,*[a,c] Yan Huang[a] and Xuemei Pu*[a]

Received 23rd February 2011, Accepted 18th April 2011
DOI: 10.1039/c1dt10305a

Four novel iridium(III) complexes bearing biphenyl (**7a–7c**) or fluorenyl (**7d**) modified benzothiazole cyclometallate ligands are synthesized. In comparison with the yellow parent complex, bis(2-phenylbenzothiozolato-$N,C^{2'}$) iridium(III) (acetylacetonate) [(**pbt**)$_2$**Ir**(**acac**)] (λ_{PLmax} = 557 nm, φ_{PL} = 0.26), **7a–7d** show 20–43 nm bathochromic shifted orange or red phosphorescence in solution, with maximum photoluminescence (PL) quantum yield of 0.62, and PL lifetime of 1.8–2.0 μs. Meanwhile, the resulting complexes also exhibit intense orange or red phosphorescence of λ_{PLmax} = 588–611 nm in solid films. The complex **7c** with two *tert*-butyl substituents possesses the highest phosphorescent efficiency both in dilute solution and thin solid films, therefore may be a prospective candidate for both doping and host emitting electrophosphorescent material. Furthermore, despite the observation of severe oxygen quenching for **7a–7d** in solution, **7a** and **7c** even show efficient emission intensity quenching by oxygen in their solid state due to the existence of void channels in crystals; consequently, they are promising molecular oxygen sensor reagents. Electrochemical measurement and DFT calculation results suggest that all these chelates own declined LUMOs of 0.1 eV relative to that of (**pbt**)$_2$**Ir**(**acac**) owing to the contribution of the phenyl substituents; whereas only **7d** shows a more destabilized HOMO (~0.1 eV) compared with the parent chelate.

Introduction

During the past twenty years, phosphorescent iridium complexes have drawn great interest due to their high quantum efficiency and color diversity, which make them promising for various applications such as phosphorescent light-emitting diodes (PhOLEDs),[1] biological labelling agents[2] and chemosensors.[3] In comparison with the well-developed green iridium complexes,[4] red ones compromising both efficiency and color purity are still scarce,[5] because the emission should originate from a smaller energy gap transition, in which more nonradiative pathways may exist from strong π–π interaction or charge transfer between ligands, hence decrease the PL quantum yield.[6] The relative poor performance of red iridium chelates has restrained their application in full color displays and biological sensors as well.

Since the excited states in Ir complexes are ligand-related, the general strategies for exploiting red phosphors are the employment of cyclometallate ligands with deliberately extended aromatic π-conjugation systems, such as 1-phenylisoquinoline (piq),[7] 2,3-diphenylquinoxaline (dbq),[8] 2-phenylbenzoquinoline (pbq),[9] 2-(2-benzo[4,5-*a*]thienyl) pyridine (btp),[10] *etc.*, and the modification on conjugated lengths of the ancillary ligands.[11] On the other hand, the emission color of Ir(III) chelates can be fine-tuned to red *via* rational modification on C^N ligands by substituents.[12] For example, Ir(III)-ppy complexes (ppy: 2-phenylpyridine) are found to have their HOMOs mainly dominated by mixtures of Ir d-orbitals and π-orbitals of phenyl moieties, consequently the addition of electron-donating groups to the phenyl segment would generally lead to red-shifted emission due to the destabilized HOMOs; whereas the LUMOs of the complexes principally localize on the π-orbitals of pyridyl groups, hence the incorporation of electron-withdrawing groups with the pyridyl moiety would mostly lead to declined LUMO, and accordingly redder emission.[13] Based on the above strategy, several red Ir-ppy type complexes have been demonstrated,[14] yet this principle is found to show some deviation in the case of both Ir-ppy analogues[15] and chelates with other C^N ligands.[16] For instance, compared with the yellow parent compound (**pbt**)$_2$**Ir**(**acac**) (λ_{PLmax} = 557 nm, φ_{PL} = 0.26),[17]

[a]*College of Chemistry, Sichuan University, Chengdu, 610064, P. R. China. E-mail: luzhiyun@scu.edu.cn; Fax: +86-28-85410059. E-mail: xmpuscu@scu.edu.cn; Fax: +86-28-85412907*
[b]*Analytical and Testing Center, Sichuan University, Chengdu, 610064, P. R. China*
[c]*Key Laboratory of Green Chemistry and Technology, Minister of Education, Sichuan University, Chengdu, 610064, P. R. China*

† Electronic supplementary information (ESI) available: Crystallographic data of **7c** and **7d** are given in CIF format and their CCDC reference numbers are 796972 and 805245. ^{1}H NMR spectra of **7a–7d** and the composition of some frontier molecular orbitals in the ground state of each complex are given in Figure S1–S5 and Table S1–S6. For ESI and crystallographic data in CIF or other electronic format see DOI: 10.1039/c1dt10305a

the addition of an electron-donating $-OCH_3$ onto the *para*-site of the phenyl of **pbt** would, however, induce a 16 nm blue-shifted PL with λ_{PLmax} of 541 nm;[16] while the alteration of the $-OCH_3$ substituent to the *meta*-position would result in a ~50 nm red-shifted PL emission (609 nm).[12] Additionally, the introduction of electron-withdrawing $-CF_3$ or –F to the *para*-site of the phenyl in **pbt** would bring 7 nm bathochromic or 16 nm hypsochromic shifts in their λ_{PLmax}, respectively.[16] Thus for **(pbt)$_2$Ir(acac)**-type complexes, the tuning of emission color through substituents on C^N ligands still relies on certain serendipitous discoveries, and the relationship between emission color and substituents has not yet been elucidated.

In pursuing Ir(III) complexes for successful electrophosphorescence or chemo/biosensor application, the other key requirement is to attain high emission quantum yields (QY). This would, inevitably, be influenced by the substituents introduced, and the collective substituent effects on φ_{PL} are not easily predicted.[18] For example, despite a few reports stating *tert*-butyl modified transition-metal chelates show slightly improved[19] or decreased[20] PLQYs in solution, our previous work has confirmed that *tert*-butylated **(pbt)$_2$Ir(acac)** exhibits remarkably enhanced solution PLQY (φ_{PL}: 0.51 *vs* 0.26).[21] Likewise, the attachment of –F, $-CF_3$, and $-OCH_3$ to C4-site of phenyl in **pbt** is also found to have positive effects on PLQY,[16] whereas the 2-(3-methoxyphenyl)benzothiazole-based analogue shows much lowered emission QY relative to that of **(pbt)$_2$Ir(acac)**.[12] Therefore, no generalized approaches have been well-established to predict the emission QY of complexes based on **(pbt)$_2$Ir(acac)** skeleton.

Although complexes bearing modified **pbt** ligands show versatile tunability for both emission color and emission QY, only a few efforts have been made to exploit efficient red **(pbt)$_2$Ir(acac)**-type phosphors.[12,22] Herewith, we report the synthesis and characterization of four novel iridium chelates with **(pbt)$_2$Ir(acac)** framework. All of them show orange or red emission in both solution and solid state, and the *tert*-butylation on phenyl is likely to benefit the enhancement of PLQY. Moreover, they all exhibit molecular oxygen quenching character in solution, and two of them even show efficient emission intensity quenching in solid state. Further investigation on electronic effects of the substituents are carried out through electrochemical experiments and theoretical computation as well.

Experimental section

General information and materials

All the chemicals commercially available were used without further purification unless otherwise stated. All the solvents were of analytical grades and freshly distilled prior to use. Anhydrous tetrahydrofuran (THF) and carbon tetrachloride were obtained by treatment with sodium and diphosphorous pentoxide, respectively, followed by distillation. ^{1}H NMR and ^{13}C NMR spectra were recorded on a Bruker AVANCE-400 spectrometer in $CDCl_3$ using TMS as internal standard. High resolution MS spectra were obtained from a Q-TOF Priemier ESI mass spectrometer (Micromass, Manchester, UK). Elemental analysis was carried out with a Carlo Erba 1106 elemental analyzer. Differential scanning calorimetry (DSC) and thermogravimetic analysis (TGA) were performed on DSC Q100 and TGA Q500 instruments, respectively, under nitrogen atmosphere at a heating rate of 10 °C min^{-1}. The purity of key intermediates and target molecules were determined by HPLC (Agilent 1100). The UV-Vis absorption spectra were acquired from 10^{-5} mol L^{-1} 2-methyltetrahydrofuran (2-MeTHF) solution on a SHIMADZU UV-2100 spectrophotometer. The photoluminescence spectra of the chelates in 10^{-5} mol L^{-1} 2-MeTHF solution and thin solid films were recorded on a HITACHI F-7000 fluorescence spectrophotometer at 298 K, while thin film samples were acquired by spin-coating from their chlorobenzene solution (10 mg mL^{-1}) at a speed of 2000 rpm on quartz substrates. PL efficiency measurements were carried out at room temperature in both argon degassed (by several freeze-pump-thaw cycles) or aerated 10^{-5} mol L^{-1} dichloromethane and 2-MeTHF solution, using 10^{-5} mol L^{-1} $Ru(bpy)_3Cl_2$ in water as the reference under excitation of 420 nm. PL lifetimes of the compounds were obtained by exponential fit of emission decay curves recorded on a FLS920 spectrofluorimeter (Edinburgh Instruments) under excitation of 440 nm at 298 K. The absolute PL quantum efficiencies of the thin films were determined with an integrating sphere (IS80 form Labsphere) together with a digital photometer (S370 from UDT) under ambient conditions, and the excitation wavelength was 440 nm. To investigate the oxygen quenching properties of the chelates in solid state, vacuum-dried crystalline samples were loaded in a rubber-stopper-equipped quartz cuvette, and the variation of PL emission intensity at λ_{PLmax} was monitored under excitation of 420 nm at a time interval of 1 s when allowing oxygen to flow over the argon-degassed samples, and the solid-state PL spectra of the complexes under pure argon and oxygen were collected with a HITACHI F-7000 fluorescence spectrophotometer. Cyclic voltammetry (CV) measurement was carried out on a PARSTAT 2273 electrochemical workstation at room temperature in argon-purged 5×10^{-4} mol L^{-1} anhydrous CH_2Cl_2 solution with tetrabutylammonium perchlorate (0.1 mol L^{-1}) as the supporting electrolyte at a scanning rate of 100 mV s^{-1}. The CV system was constructed using a platinum plate, a $Ag/AgNO_3$ (0.1 mol L^{-1} in acetonitrile) electrode and a platinum wire as the working electrode, quasi-reference electrode and counter electrode, respectively. Each measurement was calibrated with a ferrocene/ferrocenium (Fc/Fc^+) redox couple as internal standard.

X-Ray crystallographic Analysis

The crystallographic data for **7c** and **7d** reported here had been deposited in the Cambridge Database (CCDC 796972 and 805245). The determination of the unit cell and data collection for the crystals were preformed on a Rigaku Saturn CCD diffractometer or a Xcalibur E X-ray single crystal diffractometer equipped with graphite monochromator Mo-Kα ($\lambda = 0.71073$ Å) radiation. The data collection was executed using CrystalClear[23a] program for **7c** and CrysAlisPro[23b] program for **7d**. Structures were solved by direct method and successive Fourier difference syntheses (SHELXS-97), and were refined by full-matrix least-squares procedure on F^2 with anisotropic thermal parameters for all non-hydrogen atoms (SHELXL-97).[24] Packing analysis of the crystal cells was carried out using Platon,[25a] and the pictorial representations of the void spaces in the crystals were outlined with Mercury[25b] program.

Computational method

For the singlet ground states (S_0) of complexes (**pbt**)$_2$**Ir**(**acac**) and **7a–7d**, B3LYP[26] geometry optimization were performed using LANL2DZ[27] basis set for Ir and 6-31G(d) basis sets for C, H, S, N and O atoms. All the geometries were confirmed as stationary structure by the presence of only real frequencies at the same level of theory. Based on the optimized geometries, time-dependent density functional theory (TDDFT)[28] method within the framework of the IEF-PCM Model[29] in THF media was employed to calculate the lowest 20 singlet-singlet and singlet–triplet excitations at the same level. All calculations were carried out with Gaussian 09 software.[30]

Synthesis

The synthetic procedures for intermediates and objective molecules are shown in Scheme 1. 4-Bromobiphenyl (**1a**) and fluorene were available commercially from Aldrich Co., and recrystallized from ethanol before use. Intermediates **1b**,[31] **2**,[32] **3**,[33] **4a**[34] and **4b**[34] were synthesized according to the literature. The parent compound (**pbt**)$_2$**Ir**(**acac**) was synthesized following a reported procedure[17] with purity of 99.8%.

4′-Bromo-3,5-di-*tert*-butylbiphenyl (1c). To a solution of **1a** (1.0 g, 4.3 mmol) and *tert*-butyl chloride (1.2 mL, 12.8 mmol) in 10 mL of carbon tetrachloride was added 0.1 g (0.8 mmol) anhydrous aluminum chloride. The mixture was stirred at 0 °C for 4 h, then the reaction was quenched with water. The organic phase was washed with saturated sodium bicarbonate solution (2 × 50 mL), water (50 mL), and brine (50 mL) in turn, then dried over $MgSO_4$ and concentrated *in vacuo*. The resulting white solid was recrystallized from ethanol to afford white needles with yield of 46%, and purity of 99.6%. M.p.: 120–121 °C. ^{1}H NMR ($CDC1_3$, 400 MHz, δ (ppm)): 7.55 (d, J = 8.4 Hz, 2H, ArH), 7.44–7.46 (m, 3H, ArH), 7.34 (s, 2H, ArH), 1.37 (s, 18H, *t*-BuH).

Methyl 9,9-dimethyl-9*H*-fluorene-2-carboxylate (3). To a solution of 9,9-dimethyl-9*H*-fluorene (**2**) (1.0 g, 5.15 mmol) and oxalyl

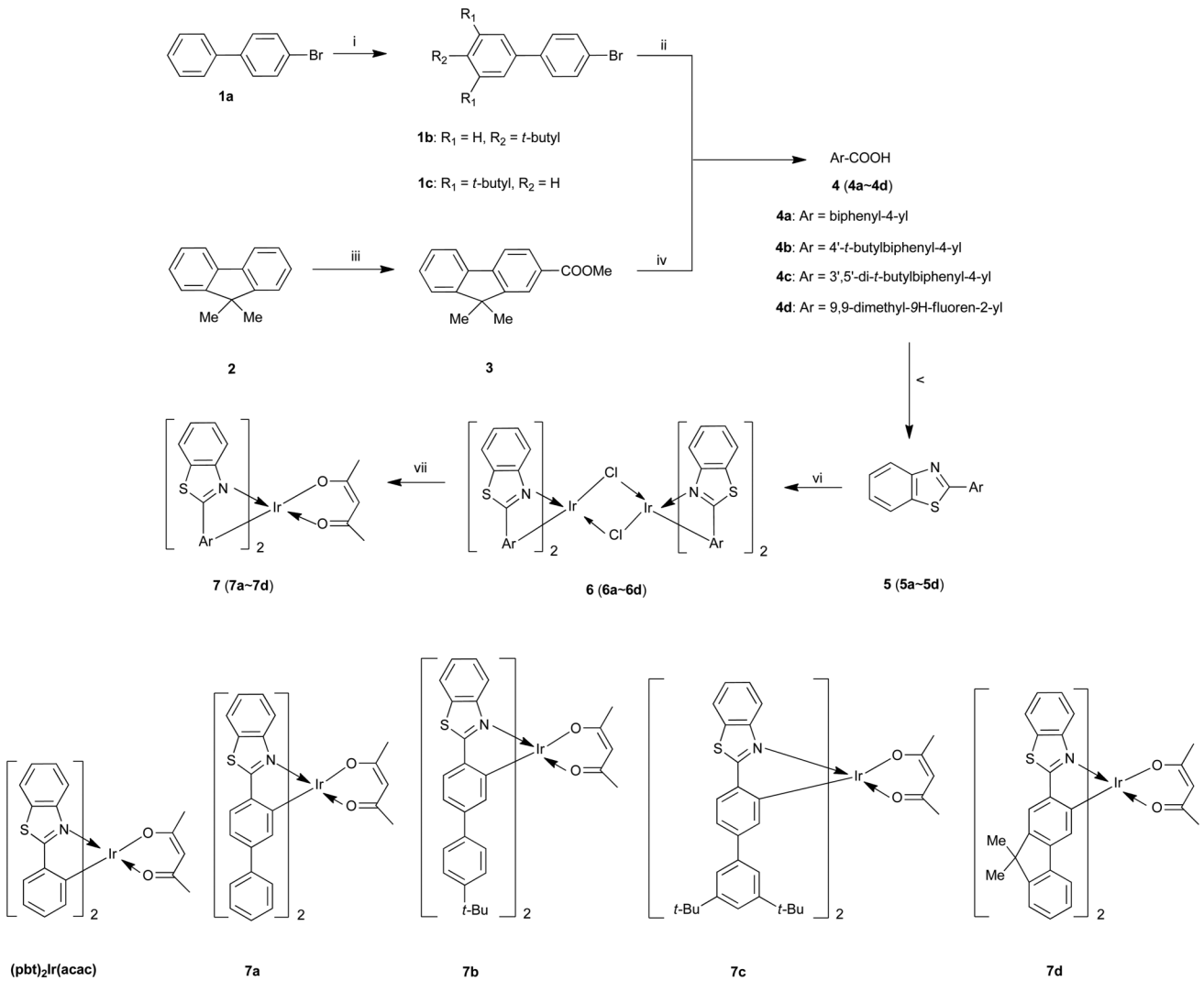

Scheme 1 The synthetic routes of the objective iridium(III) complexes, and the sketch map of the five chelates studied here as well. Reagents and reaction conditions for the synthetic procedures: (i) $(CH_3)_3CCl$, $AlCl_3$, CCl_4, 0 °C; (ii) (a) Mg, THF, reflux, (b) CO_2, H^+; (iii) (a) $(COCl)_2$, CH_2Cl_2, $AlCl_3$, 0 °C, (b) CH_3OH, CH_2Cl_2; (iv) CH_3OH, THF, KOH, reflux; (v) (a) $SOCl_2$, reflux, (b) *o*-aminothiophenol, NMP, 100 °C; (vi) $IrCl_3 \cdot nH_2O$, 2-ethoxyethanol (aq), 110 °C; (vii) acetylacetone, 2-ethoxyethanol, Na_2CO_3, 110 °C.

chloride (1.29 g, 10.3 mmol) in 10 mL dichloromethane was added 2.04 g (15.45 mmol) of aluminum chloride at 0 °C. After stirring for 4 h, the mixture was poured into 100 mL water with crushed ice followed by extraction with ethyl acetate (3 × 20 mL). The organic layer was washed with brine, dried over Na_2SO_4, then the solvent was removed to yield white residue. It was dissolved into 40 mL dichloromethane and 10 mL methanol, followed by 2 h stirring at room temperature, then concentrated *in vacuo*. The crude product was purified by column chromatography to afford white solid (eluent: dichloromethane/*n*-hexane = 1/1), yield: 78%. ^{1}H NMR ($CDCl_3$, 400 MHz, δ (ppm)): 8.11 (s, 1H, ArH), 8.05 (d, J = 8 Hz, 1H, ArH), 7.78–7.75 (m, J = 4 Hz, 2H, ArH), 7.47 (t, J = 3.6 Hz, 1H, ArH), 7.37 (t, J = 4 Hz, 2H, ArH), 3.96 (s, 3H, MeH), 1.52 (s, 6H, MeH).

3′,5′-Di-*tert*-butylbiphenyl-4-carboxylic acid (4c). 3′,5′-Di-*tert*-butylbiphenyl magnesium bromide was prepared from **1c** (3.44 g, 10 mmol) with magnesium (0.27 g, 11 mmol), then reacted with 10 g dry ice followed by treatment with 1 mol L^{-1} hydrochloric acid to yield white precipitate. The crude product was recrystallized from hexane to afford white needles. Yield: 54%; ^{1}H NMR ($CDCl_3$, 400 MHz, δ (ppm)): 8.20 (d, J = 8.4 Hz, 2H, ArH), 7.70 (d, J = 8.4 Hz, 2H, ArH), 7.50 (s, 1H, ArH), 7.47 (s, 2H, ArH), 1.37 (s, 18H, *t*-BuH).

9,9-Dimethyl-9*H*-fluorene-2-carboxylic acid (4d). A solution of **3** (2.52 g, 10 mmol) in hot methanol (20 mL) and THF (20 mL) was added into 30 mL 1 mol L^{-1} aqueous KOH. The mixture was refluxed for 3 h, then neutralized by concentrated hydrochloric acid to pH = 1.0. The white precipitate was collected and recrystallized from methanol. Yield: 88.6%.

General procedure for the synthesis of cyclometallate ligands 5a–5d[16]. 10 mmol of carboxylic acid (**4**) was refluxed with 20 mL thionyl chloride for 3 h, then excessive thionyl chloride was removed *in vacuo*. The residue was dissolved in 20 mL *N*-methylpyrrolidinone (NMP), then added dropwise into a solution of 10 mmol of *o*-aminothiophenol in 20 mL NMP under inert atmosphere, followed by stirring at 100 °C for 1 h. After cooled down, the reactant was poured into water followed by neutralization with 7 mol L^{-1} aqueous ammonia to pH = 8~9. The precipitate was filtered and recrystallized from alcohol to afford intermediate **5**.

2-(4′-*tert*-Butylbiphenyl-4-yl)benzo[*d*]thiazole (5b). White plate crystal. Yield: 74.6%; m.p.: 217–220 °C; ^{1}H NMR ($CDCl_3$, 400 MHz, δ (ppm)): 8.15 (d, J = 8 Hz, 2H, ArH), 8.08 (d, J = 8 Hz, 1H, ArH), 7.91 (d, J = 8 Hz, 1H, ArH), 7.72 (d, J = 8.4 Hz, 2H, ArH), 7.61 (d, J = 8.4 Hz, 2H, ArH), 7.41–7.51 (m, 3H, ArH), 7.39 (t, J = 8 Hz, 1H, ArH), 1.37 (s, 9H, *t*-BuH).

2-(3′,5′-Di-*tert*-butylbiphenyl-4-yl)benzo[*d*]thiazole (5c). White needles. Yield: 68.6%; m.p.: 165–167 °C; ^{1}H NMR ($CDCl_3$, 400 MHz, δ (ppm)): 8.16 (d, J = 8 Hz, 2H, ArH), 8.10 (d, J = 8 Hz, 1H, ArH), 7.91 (d, J = 7.6 Hz, 1H, ArH), 7.72 (d, J = 8.4 Hz, 2H, ArH), 7.47–7.52 (m, 4H, ArH), 7.39 (t, J = 8 Hz, 1H, ArH), 1.40 (s, 18H, *t*-BuH).

2-(9,9-Dimethyl-9*H*-fluoren-2-yl)benzo[*d*]thiazole (5d). Yellow column crystal. Yield: 78.6%; m.p.: 134–137 °C; ^{1}H NMR ($CDCl_3$, 400 MHz, δ (ppm)): 8.23 (s, 1H, ArH), 8.11 (d, J = 8.4 Hz, 1H, ArH), 8.06 (d, J = 0.4 Hz, 1H, ArH), 8.04 (d, J = 0.8 Hz, 1H, ArH), 7.92 (d, J = 8 Hz, 1H, ArH), 7.82 (d, J = 8 Hz, 1H, ArH), 7.77–7.79 (m, J = 8 Hz, 1H, ArH), 7.52–7.46 (m, J = 2.4 Hz, 1H, ArH), 7.41–7.36 (m, J = 2 Hz, 3H, ArH), 1.58 (s, 6H, MeH).

General procedure for the synthesis of target iridium(III) complexes 7a–7d. Dichloro-bridged iridium(III) complexes (**6a–6d**) were prepared by refluxing $IrCl_3 \cdot nH_2O$ (1 mmol) with cyclometallate ligands **5** (2.4 mmol) in a mixture of 2-ethoxyethanol and water (3 : 1) under argon for 24 h.[35] The precipitate was filtered and washed with 10 mL of 1 mol L^{-1} HCl and 3 × 15 mL methanol in sequence, then dried over *vacuo* to afford **6**. Target compounds of **7a–7d** were prepared by refluxing the chloride-bridged dimers **6** (0.1 mmol), acetylacetone (0.3 mmol) and sodium carbonate (1 mmol) in 10 mL of 2-ethoxyethanol under argon for 12 h. After cooled down, the precipitates were collected and purified from flash chromatography through silica column using $CHCl_3$ as eluent, followed by more than three times recrystallization procedure to afford satisfied purity, then dried for 24 h at 100 °C under vacuum of 1.5 kPa.

Bis[2-(biphenyl-4-yl)benzothiazolato-*N*,*C*$^{2'}$]iridium(III)(acetylacetonate) (7a). Red solid, recrystallized from a mixture of benzene and methanol. Yield: 45%; purity: 98.9%. ^{1}H NMR ($CDCl_3$, 400 MHz, δ (ppm)): 8.17 (d, J = 3.6 Hz, 1H, ArH), 8.16 (s, 1H, ArH), 7.92 (s, 1H, ArH), 7.90 (d, J = 3.6 Hz, 1H, ArH), 7.70 (d, J = 7.6 Hz, 2H, ArH), 7.45 (t, J = 4.6 Hz, 4H, ArH), 7.14–7.18 (m, 10H, ArH), 7.08 (d, J = 8 Hz, 2H, ArH), 6.62 (s, 2H, ArH), 5.16 (s, 1H, acacH), 1.79 (s, 6H, acacH). ^{13}C NMR (100 MHz, $CDCl_3$, δ (ppm)): 185.81, 179.83, 150.94, 148.54, 142.17, 141.30, 141.23, 133.45, 131.45, 128.31, 127.33, 127.26, 127.20, 127.05, 125.99, 125.11, 122.36, 120.81, 120.20, 101.70, 28.40. TOF-MS: m/z 887.1354 (M + Na^+); Calcd for M_w + Na^+: 887.1342. Anal. Calcd for $C_{43}H_{31}IrN_2O_2S_2$: C, 60.05; H, 3.74; N, 3.19; S, 7.28. Found: C, 59.77; H, 3.62; N, 3.24; S, 7.42.

Bis[2-(4′-*tert*-butylbiphenyl-4-yl)benzothiazolato-*N*,*C*$^{2'}$]iridium(III)(acetylacetonate) (7b). Red solid. It was purified by recrystallization from a mixture of dichloromethane and benzene, and may contain 1 : 1 cocrystallized benzene even after drying in vacuum. Yield: 30%; purity: 99.2%. ^{1}H NMR ($CDCl_3$, 400 MHz, δ (ppm)): 8.14–8.17 (m, 2H, ArH), 7.90–7.92 (m, 2H, ArH), 7.67 (d, J = 8 Hz, 2H, ArH), 7.44–7.47 (m, 4H, ArH), 7.20–7.22 (d, 4H, ArH), 7.36 (s, ~5H, ArH of benzene), 7.06–7.10 (m, 6H, ArH), 6.64 (s, 2H, ArH), 5.15 (s, 1H, acacH), 1.79 (s, 6H, acacH), 1.25 (s, 18H, *t*-BuH). ^{13}C NMR (100 MHz, $CDCl_3$, δ (ppm)): 185.83, 179.98, 151.07, 150.09, 148.56, 142.04, 141.12, 138.33, 133.32, 131.51, 128.41, 127.31, 126.93, 126.09, 125.35, 125.05, 122.40, 120.72, 120.23, 101.73, 34.46, 31.37, 28.40. TOF-MS: m/z 999.2588 (M + Na^+); Calcd for M_w + Na^+: 999.2606. Anal. Calcd. for $C_{51}H_{47}IrN_2O_2S_2 \cdot C_6H_6$: C, 64.81; H, 5.14; N, 2.63; S, 5.98. Found: C, 64.93; H, 5.07; N, 2.66; S, 6.08.

Bis[2-(3′,5′-di-*tert*-butylbiphenyl-4-yl)benzothiazolato-*N*,*C*$^{2'}$]iridium(III)(acetylacetonate) (7c). Red solid, recrystallized from a mixture of benzene and methanol. Yield: 36%; purity: 98.9%. ^{1}H NMR ($CDCl_3$, 400 MHz, δ (ppm)): 8.22 (d, J = 8.4 Hz, 2H, ArH), 7.86 (d, J = 8 Hz, 2H, ArH), 7.65 (d, J = 7.6 Hz, 2H, ArH), 7.41–7.52 (m, 4H, ArH), 7.25 (s, 2H, ArH), 7.10 (d, J = 8 Hz, 2H, ArH), 7.00 (s, 4H, ArH), 6.62 (s, 2H, ArH), 5.19 (s, 1H, acacH), 1.82 (s, 6H, acacH), 1.16 (s, 36H, *t*-BuH). ^{13}C NMR (400 MHz, $CDCl_3$, δ (ppm)): 185.78, 179.87, 151.05, 150.43,

Table 1 Crystal data and structure refinement for complex **7c** and **7d**

Compounds	**7c**	**7d**
Empirical formula	$C_{71}H_{75}IrN_2O_2S_2{\cdot}2C_6H_6$	$C_{49}H_{40}IrN_2O_2S_2$
Formula weight	1244.65	944.14
Temperature	113(2) K	150(2) K
Wavelength	0.71073 Å	0.71073 Å
Crystal system	Triclinic	Triclinic
Space group	$P\bar{1}$	$P\bar{1}$
a	11.046(2) Å	12.028(13) Å
b	15.200(3) Å	13.348(17) Å
c	18.650(4) Å	17.714(2) Å
α	88.90(3) deg	95.58(11) deg
β	81.91(3) deg	96.78(10) deg
γ	87.03(3) deg	102.79(10) deg
Volume	3095.8(11) Å^3	2731.6(6) Å^3
Z	2	2
Calculated density	1.335 mg m^{-3}	1.148 mg m^{-3}
Absorption coefficient	2.270 mm^{-1}	2.552 mm^{-1}
F(000)	1280	944
Crystal size	0.20 × 0.18 × 0.10 mm	0.42 × 0.40 × 0.35 mm
Reflections collected	22776	23069
Independent reflections	10867 [*R*(int) = 0.0325]	11108 [*R*(int) = 0.0273]
θ-range for data collection	1.73 to 25.02°	2.98 to 26.37°
Goodness-of-fit on F^2	1.065	1.092
Final *R* indices [$I > 2\sigma(I)$]	$R_1 = 0.0269$, w$R_2 = 0.0647$	$R_1 = 0.0297$, w$R_2 = 0.0767$
R indices (all data)	$R_1 = 0.0295$, w$R_2 = 0.0665$	$R_1 = 0.0341$, w$R_2 = 0.0792$
Largest diff. peak and hole	1.063 and −1.763 e·Å^{-3}	0.819 and −0.674 e·Å^{-3}

148.66, 143.18, 140.87, 140.14, 133.67, 131.46, 127.37, 125.90, 125.11, 122.24, 121.70, 121.15, 120.51, 120.24, 101.73, 34.76, 31.39, 28.45. TOF-MS: *m*/*z* 1089.3977 (*M* + H$^+$); Calcd for M_w + H$^+$: 1089.3960. Anal. Calcd for $C_{59}H_{63}IrN_2O_2S_2$: C, 65.35; H, 5.92; N, 2.53; S, 5.95. Found: C, 65.10; H, 5.83; N, 2.57; S, 5.89.

Bis[2-(9,9-dimethyl-9*H*-fluoren-2-yl)benzothiazolato-*N*,*C*$^{2'}$]iridium(III)(acetylacetonate) (7d). Red solid, recrystallized from a mixture of chloroform and methanol. Yield: 42%; purity: 99.2%. ^{1}H NMR ($CDCl_3$, 400 MHz, δ (ppm)): 8.13 (s, 1H, ArH), 8.11 (d, *J* = 4 Hz, 1H, ArH), 7.97 (d, *J* = 4 Hz, 1H, ArH), 7.96 (s, 1H, ArH), 7.67 (s, 2H, ArH), 7.45 (t, *J* = 4 Hz, 4H, ArH), 7.28 (d, *J* = 7.6 Hz, 2H, ArH), 7.12–7.16 (m, 2H, ArH), 7.08 (s, 4H, ArH), 6.74 (s, 2H, ArH), 5.18 (s, 1H, acacH), 1.79 (s, 6H, acacH), 1.46 (s, 6H, CH_3), 1.40 (s, 6H, CH_3). ^{13}C NMR (100 MHz, $CDCl_3$, δ (ppm)):185.81, 180.32, 154.85, 151.15, 146.99, 146.89, 141.51, 140.70, 138.62, 131.20, 127.53, 127.42, 126.43, 125.94, 124.89, 122.27, 120.40, 120.24, 120.06, 101.80, 46.08, 28.48, 27.45, 27.31. TOF-MS: *m*/*z* 945.1849 (*M* + H$^+$); Calcd for M_w + H$^+$: 945.2160. Anal. Calcd for $C_{49}H_{39}IrN_2O_2S_2$: C, 62.33; H, 4.16; N, 2.97; S, 6.79. Found: C, 62.80; H, 4.01; N, 2.97; S, 6.61.

Results and discussion

Synthesis and characterization

All these heteroleptic complexes are synthesized from reaction of $IrCl_3{\cdot}nH_2O$ with cyclometallate ligands to form chloride-bridged complexes $[(C^N)_2IrCl]_2$, followed by treatment with acetylacetone. The synthetic routes are outlined in Scheme 1. The key intermediates of carboxylic acids for C^N ligands are prepared through Grignard reaction in the case of **4a–4c**, and Friedel–Crafts acylation for **4d**; while the aryl bromides **1b** and **1c** are prepared by Friedel–Crafts *tert*-butylation using **1a** as reactant. It is noteworthy that **1c** just exists as byproduct initially with poor yield of 12% in the procedure for preparing **1b**,[31] while the reaction conditions are optimized with prolonged reaction time and excessive feeding ratio of anhydrous $AlCl_3$ to achieve a much improved yield of 46% finally.

Single crystals of complex **7c** and **7d** are obtained from slow vapor diffusion of methanol into their benzene or $CHCl_3$ solution, and 2 equivalent crystallized benzene molecules can be found in the unit cell of **7c**. The crystallographic refinement parameters, selected bond distances as well as bond angles of **7c** and **7d** are summarized in Table 1 and 2, respectively, and their crystal structures are shown in Fig. 1. It is clear that both the two complexes reveal

Table 2 Selected bond lengths (Å) and angles (deg) for **7c** and **7d**

Bond lengths (Å)		Bond angles (deg)	
7c			
Ir(1)–C(13)	1.992(3)	C(13)–Ir(1)–N(2)	95.01(10)
Ir(1)–C(40)	1.992(3)	C(40)–Ir(1)–N(1)	94.70(11)
Ir(1)–N(1)	2.045(2)	N(2)–Ir(1)–O(1)	88.10(8)
Ir(1)–N(2)	2.044(2)	N(2)–Ir(1)–N(1)	173.20(8)
Ir(1)–O(1)	2.1573(19)	N(1)–Ir(1)–O(1)	96.34(8)
Ir(1)–O(2)	2.131(2)	O(2)–Ir(1)–O(1)	87.84(8)
O(1)–C(56)	1.270(3)	N(2)–Ir(1)–O(2)	99.14(9)
O(2)–C(58)	1.266(3)	N(1)–Ir(1)–O(2)	86.20(9)
7d			
Ir(1)–C(14)	2.001(3)	C(14)–Ir(1)–N(2)	93.39(12)
Ir(1)–C(47)	1.993(3)	C(47)–Ir(1)–N(1)	93.60(12)
Ir(1)–N(1)	2.058(3)	N(2)–Ir(1)–O(1)	101.64(10)
Ir(1)–N(2)	2.055(3)	N(2)–Ir(1)–N(1)	171.16(10)
Ir(1)–O(1)	2.158(2)	N(1)–Ir(1)–O(1)	84.78(10)
Ir(1)–O(2)	2.155(2)	O(2)–Ir(1)–O(1)	87.40(9)
O(1)–C(1)	1.267(4)	N(2)–Ir(1)–O(2)	86.57(10)
O(2)–C(3)	1.272(4)	N(1)–Ir(1)–O(2)	99.90(10)

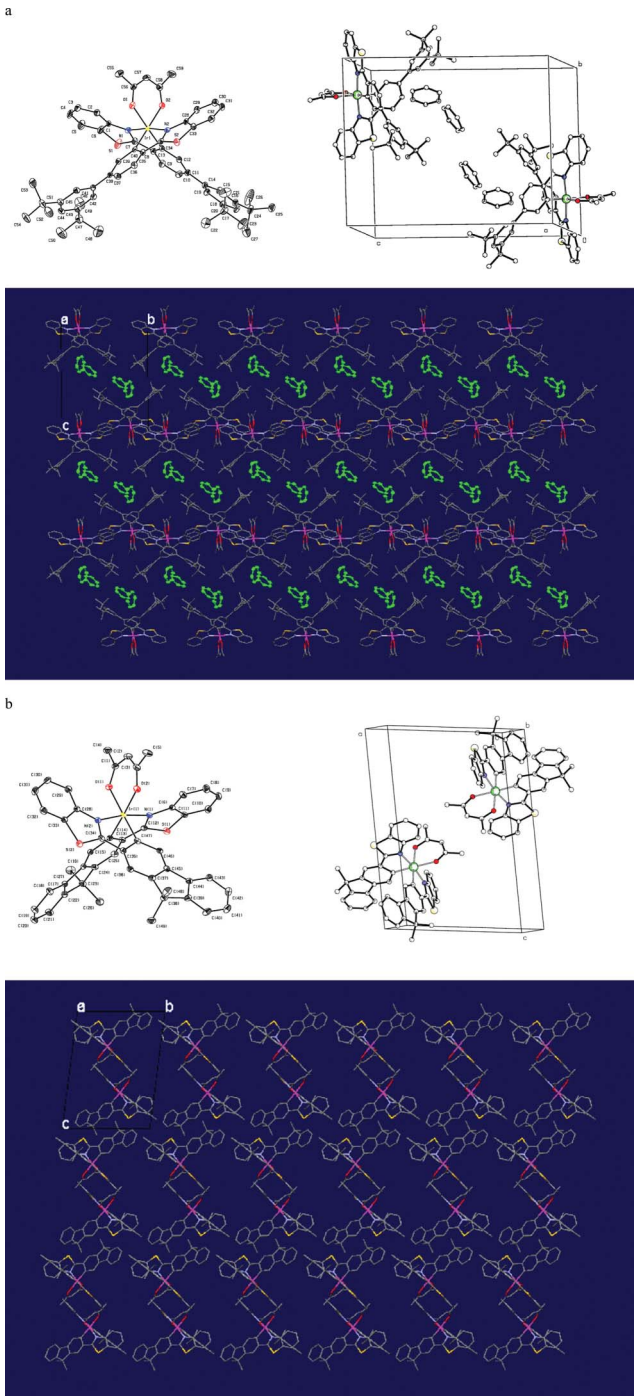

Fig. 1 The **ORTEP** drawing, crystal cell structure and packing diagram viewed down the *a* axis of crystal structures of **7c** (a) and **7d** (b).

distorted octahedral geometries around the Ir atom with the two C^N ligands adopting C,C-*cis*, N,N-*trans* configurations, which are akin to those for analogous iridium complex $(tbt)_2Ir(acac)$ {tbt: 2-(*p*-tolyl)benzo[*d*]thiazole}.[36] In **7d**, the bond lengths of the two Ir–O bonds are almost identical, while in the case of **7c**, they differed slightly from each other [2.131(2) and 2.1573(19) Å], suggesting the phenyl groups in **7c** exist *trans*-influence.[36] The dihedral angles between the benzothiazole and the aryl rings are 9.99 (0.11)° and 14.49 (0.12)° for **7c**, while 8.50 (0.14)° and 18.71 (0.14)° for **7d**, both are larger than those observed in $(tbt)_2Ir(acac)$, implying **7c** and **7d** have less efficient π-conjugation system relative to $(tbt)_2Ir(acac)$.[37] The biphenyl moieties in **7c** exhibit twisted geometry with dihedral angles of 33.59 (0.14)° and 44.72 (0.14)°, while in the case of **7d**, the dihedral angles between the two phenyl in fluorenyl are 9.11 (0.18)° and 2.35 (0.17)°. Thus **7d** bearing one nearly coplanar C^N ligands should have more extended conjugation system. Additionally, spacious cavities accommodating four benzene molecules can be observed between two neighboring molecules of **7c** in the crystal cell (*vide* Fig. 1a), validating that **7c** possesses a bulky volume. Consequently, the molecular aggregation and concentration quenching of **7c** could be reduced effectively in its solid state.

Examination of the molecular packing of the structures of **7c** shows the existence of narrow channels containing two cocrystallized benzene molecules per Ir unit. It was speculated that if the crystals of **7c** could lose all solvents without loss of crystallinity, more void spaces would be released after removal of benzene to form open vacant channels which may allow the diffusion of small molecules such as oxygen into and out of the crystals, hence enable efficient emission quenching in crystalline form.[38] While in the case of **7d**, only small isolated voids could be found (*vide* Fig. 1b), so we expect it has less oxygen sensing character in comparison with **7c**.

Thermal properties

DSC results reveal that all the complexes show decomposition prior to melting transition with no obvious glass transition peaks. TGA of the complexes indicates that all of the compounds are stable in air without crystallized solvent molecules except for **7b**, and their decomposition temperatures (at 5 wt% loss) are determined as 318~362 °C, suggesting that they have good thermostability (thermograms and data are shown in Fig. 2 and Table 4). It is worthy of note that the initial weight loss of ~7% at 254 °C of **7b** should be due to the loss of benzene from **7b**·benzene (1 : 1) complex that is formed in the recrystallization procedure, which can be further confirmed by the elementary analysis data and ^1H NMR spectrum (the intense signal at $\delta = 7.36$ ppm, *vide* ESI Figure S2,† the sample has been dried for 24 h at 100 °C under vacuum of 1.5 kPa before the measurement). Interestingly, although the X-ray crystallographic analysis of **7c** shows two equiv. of crystallized benzene in its unit cell, no analogous

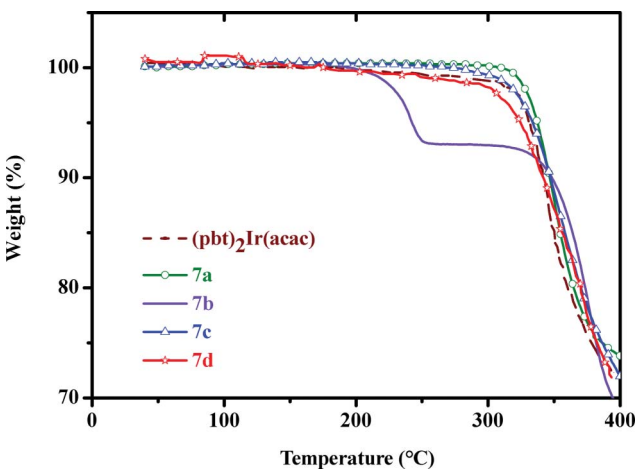

Fig. 2 TGA thermograms of $(pbt)_2Ir(acac)$ and **7a–7d**.

Table 3 Photophysical data of the complexes studied here

Compound	Absorbance λ_{max} (nm) (log ε)[a]	λ_{PLmax} (nm) solution[b]	λ_{PLmax} (nm) film[c]	φ_{PL}[b]	φ_{PL}(%)[e]	lifetime τ (μs)[d]	k_r (s^{-1})[e]	k_{nr} (s^{-1})[e]	$k_q[O_2]$ (s^{-1})[f]
(pbt)$_2$Ir(acac)	313(4.4), 327(4.5), 358(3.9), 447(3.7), 488(3.6)	557	584	0.26 (0.06)	0.47	1.8 (0.08)	1.44×10^5	4.11×10^5	1.18×10^7
7a	311(4.7), 331(4.8), 341(4.8), 417(4.0), 464(3.9), 501(3.8)	578	598, 634sh	0.24 (0.03)	0.75	1.8 (0.13)	1.33×10^5	4.22×10^5	0.75×10^7
7b	313(4.6), 344(4.7), 417(4.0), 463(3.8), 501(3.6)	578	593	0.33 (0.04)	1.13	1.9 (0.12)	1.74×10^5	3.53×10^5	0.80×10^7
7c	313(4.5), 344(4.7), 418(4.0), 465(3.8), 503(3.7)	577	588	0.62 (0.04)	1.77	2.0 (0.15)	3.10×10^5	1.90×10^5	0.64×10^7
7d	322(4.5), 355(4.7), 425(4.1), 478(3.8), 516(3.7)	600	611	0.33 (0.02)	0.47	2.0 (0.11)	1.65×10^5	3.35×10^5	0.89×10^7

[a] UV-Vis absorbance is determined in 10^{-5} mol L^{-1} 2-MeTHF solution at 298 K. [b] PL emission spectra are acquired in argon degassed 10^{-5} mol L^{-1} 2-MeTHF solution. PL efficiencies in deaerated 10^{-5} mol L^{-1} dichloromethane and as delivered 2-MeTHF solution (values in parenthesis) are determined using $Ru(bpy)_3Cl_2$ as the standard (φ = 0.042 and 0.028 in deaerated and as delivered water solution)[41] under excitation of 420 nm. [c] Thin films are spin-coated from 10 mg mL^{-1} chlorobenzene solution, PL spectra are obtained under irradiation of 420 nm. The absolute PL quantum yields of the compounds in thin solid films are measured in an intergrating sphere under ambient conditions. [d] Lifetime is determined in argon degassed and as delivered (values in parenthesis) 10^{-5} mol L^{-1} 2-MeTHF solution. [e] The radiative and overall nonradiative constants k_r and k_{nr} are calculated through the equition $k_r = \varphi_{PL}/\tau$ and $k_{nr} = (1 - \varphi_{PL})/\tau$.[42] [f] Oxygen quenching rates are determined in as delivered 10^{-5} mol L^{-1} 2-MeTHF solution, which are calculated from the equation $k_q[O_2] = (1 - \varphi)/\tau$.[44]

Table 4 Electrochemical and thermal data of the iridium complexes

Compound	$E_{1/2}^{ox}$ (V)[a,b]	E_g (eV)[c]	HOMO (eV)[d]	LUMO (eV)[e]	HOMO (eV)[f]	LUMO (eV)[f]	T_d (°C)[g]
(pbt)$_2$Ir(acac)	0.51	2.23	−5.31	−3.08	−5.28	−1.80	326
7a	0.49	2.13	−5.29	−3.16	−5.29	−1.91	355
7b	0.50	2.12	−5.30	−3.18	−5.27	−1.89	353
7c	0.49	2.12	−5.29	−3.17	−5.26	−1.87	362
7d	0.41	2.07	−5.21	−3.16	−5.17	−1.91	318

[a] Oxidation potential values are measured in CH_2Cl_2 solution containing 5×10^{-4} mol L^{-1} of the iridium(III) complexes. [b] $E_{1/2}^{ox} = 1/2(E_p^a + E_p^c)$, potential values are reported *versus* Fc/Fc^+. [c] E_g are estimated from the onset wavelength of the optical absorption bands. [d] HOMO energies are deduced from the equation HOMO = 4.8 + $E_{1/2}^{ox}$. [e] LUMO energies obtained from the equation LUMO = HOMO + E_g. [f] Obtained from B3LYP calculations within the framework of the IEF-PCM model in THF media. [g] Temperature with 5 wt% loss (12 wt% loss in the case of **7b**).

benzene complex is obtained after vacuum drying at 100 °C. These observations give a clue that complex **7b** with tightly held benzene molecules should have smaller void spaces relative to **7c**, therefore it is expected to exhibit less efficient oxygen quenching property.

Photophysical data

All these Ir(III) complexes exhibit two distinguishable absorption bands in UV-Vis region. The intense ones in 300~380 nm with log $\varepsilon > 4$ are generally assigned to the spin-allowed $^1(\pi–\pi^*)$ transition due to the contributions from cyclometallate ligands,[39] while the weaker low energy features at 420~550 nm are generally ascribed to the metal to ligand charge-transfer (^{1}MLCT and ^{3}MLCT) and the spin–orbit coupling enhanced $^3(\pi–\pi^*)$ transition.[40] The absorption curves of **7a–7d** resemble one another in shape, yet differ slightly from that of **(pbt)$_2$Ir(acac)**, implying **7a–7d** may have similar excitation characters. It can be seen from Fig. 3 and Table 3 that **7a–7d** show bathochromic absorption relative to that of **(pbt)$_2$Ir(acac)** in both the two major bands, and **7d** exhibits the most red-shifted ones. Thus the replacement of phenyl into biphenyl in C^N ligands would result in comparatively narrow band gap, while the fluorenyl group would bring about the most extended conjugation system for the chelate.

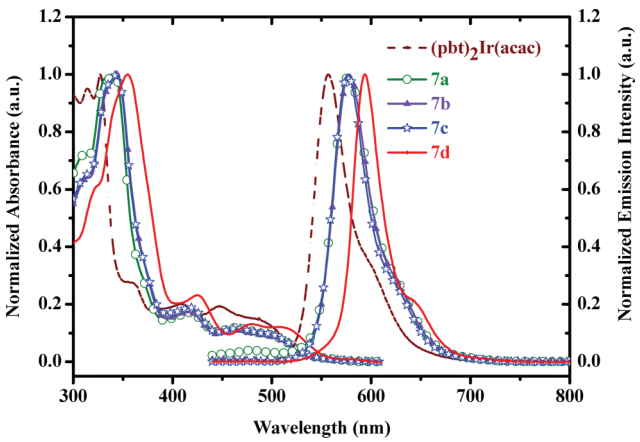

Fig. 3 Normalized absorption and PL spectra of the iridium complexes studied here in 10^{-5} mol L^{-1} 2-MeTHF solution at 298 K. PL spectra are obtained under irradiation of 420 nm.

All these iridium complexes exhibit intense orange/red phosphorescence in solution at room temperature. In accordance with the UV-Vis absorption spectra, the λ_{PLmax} of **7a**, **7b** and **7c** (~578 nm) red-shift for 20 nm relative to **(pbt)$_2$Ir(acac)**; while complex **7d** possesses the reddest phosphorescence with PL peak at

600 nm. PLQY of **(pbt)$_2$Ir(acac)** in argon-degassed dilute solution is determined as 0.26, which is consistent with the literature report (using *fac*-Ir(ppy)$_3$ as standard reference).[17] Its phenyl-modified derivative **7a** shows a φ_{PL} of 0.24; whilst **7b** and **7c** bearing bulky *tert*-butyl modified cyclometallate ligands have enhanced φ_{PL} of 0.33 and 0.62, respectively; and that of **7d** with rigid fluorenyl is calculated to be 0.33. As the five chelates possess analogical triplet lifetime (1.8~2.0 μs) in solution, the radiative and nonradiative rate constants k_r and k_{nr} of **(pbt)$_2$Ir(acac)**, **7a**, **7b** and **7d**, calculated from the equations $k_r = \varphi_{PL}/\tau$ and $k_{nr} = (1 - \varphi_{PL})/\tau$,[42] are quite similar, whereas **7c** owns much higher k_r and lower k_{nr}, simultaneously. Because **7a–7c** have much resembled PL spectra in solution, which indicates *tert*-butyl may contribute little electronic effect to the radiative decay processes, the favorable PL efficiency of **7c** may be attributed to the reduction of the interaction of the luminescent parts of molecules.[43]

In comparison with those determined in degassed solution, the φ_{PL} of **7a–7d** in their air-saturated solutions drop greatly to 0.02~0.04, and the lifetime is shortened dramatically to 0.08~0.15 μs as well, therefore the deteriorated PLQYs are ascribed to triplet oxygen quenching. The oxygen quenching rate of these chelates, based on the equation[44] $k_q[O_2] = (1 - \varphi)/\tau$, are calculated to be 0.64~1.18 × 10^7 s^{-1}. Since the lifetime, PLQY and $k_q[O_2]$ of our target molecules are comparable to those of Ir(ppy)$_3$,[44] which has been demonstrated successfully to be the first Ir-complex oxygen sensor,[45] our complexes **7a–7d** are prospective phosphorescent chemosensor reagents for dissolved oxygen measurement in solution or polymer dispersed matrices.

To investigate their potential use as non-doping host phosphors in PhOLEDs, and solid molecular oxygen sensors as well, solid-state emission spectra of **7a–7d** are acquired (shown in Fig. 4). Similar to those observed in solution, **7a–7d** display red-shifted PL spectra compared with their prototype in solid films with λ_{PLmax} of 588~611 nm, each accompanied with a shoulder peak tailing to the lower energy region, and their emission colors range from orange to red. The PL spectra collected from solid films are broader with more bathochromic effect relative to those acquired from solution, which may be due to the aggregation of phosphorescent chromophores.[46] It is found that **(pbt)$_2$Ir(acac)** owns the largest difference of 27 nm between the λ_{PLmax} in solution and film, while those for **7a–7d** are 20 nm, 15 nm, 11 nm and 11 nm, successively, hence **7a–7d** should possess less molecular stacking.

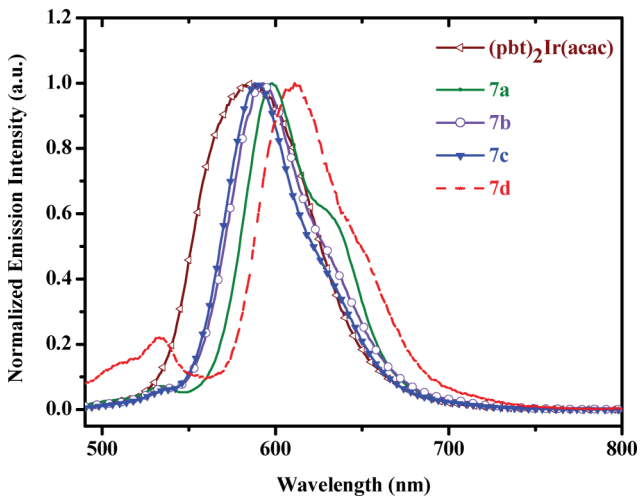

Fig. 4 Phosphorescence spectra of the iridium complexes in thin solid films at 298 K (under irradiation of 420 nm).

Though in most cases, no severe triplet oxygen quenching could be observed in the solid state of phosphorescent complexes owing to the immobilization of dissolved oxygen,[38a,44] the spacious void channels found in the crystal structure of **7c** evokes our interest to investigate emission intensity quenching character of the target compounds (depicted in Fig. 5). Surprisingly, all five complexes show some emission quenching in oxygen relative to argon, and the intensity quenched fraction $(I_0 - I)/I_0$ for **7c** (λ_{PLmax} = 594 nm), as expected, is the highest among all these compounds [$(I_0 - I)/I_0 = 0.68$]; that of **7b** which has smaller void spaces due to the existence of tightly cocrystallized benzene is much lower [$(I_0 - I)/I_0 = 0.28$];. while that of **7d** possessing isolated small voids is as low as 0.19. Interestingly, **7a** exhibits a rather high intensity quenched fraction [$(I_0 - I)/I_0$] of 0.57 and **(pbt)$_2$Ir(acac)** also shows some quenching character with [$(I_0 - I)/I_0$] of 0.23. Thus the distorted biphenyl moiety should be the key component for constructing porous crystalline iridium complexes. This is, to our knowledge, the first report on the discovery of iridium complexes that show efficient emission intensity quenching by oxygen in condensed solid states. As these compounds show intense PL in solid state, they have promising application as crystalline oxygen sensors.

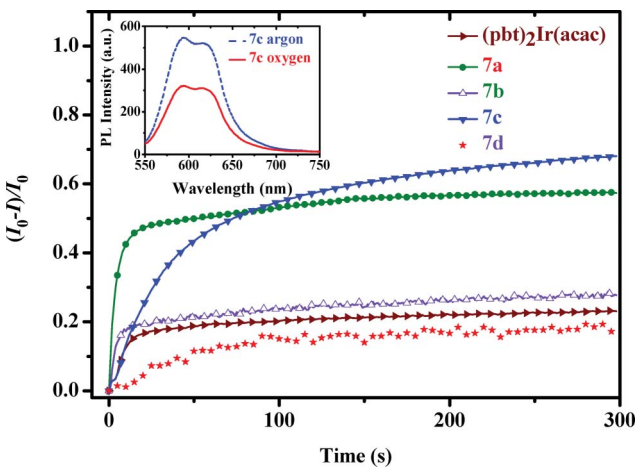

Fig. 5 Plot of $(I_0 - I)/I_0$ *vs* time for the argon predegassed crystalline samples under oxygen purging. I_0 represents the intensity of λ_{PLmax} of each compound in argon; while I is that of oxygen purged sample. The λ_{PLmax} monitored for **(pbt)$_2$Ir(acac)**, **7a–7d** is 591, 599, 600, 594 and 613 nm, consecutively. The inset figure depicts the emission spectra of solid complex **7c** under argon and air, showing the quenching of the emission in the presence of oxygen.

As far as absolute quantum efficiency in solid films is concerned, **(pbt)$_2$Ir(acac)** and **7d** have relatively low QYs of 0.47%; **7a** bearing twisted geometry has an increased QY of 0.75%; while **7b** and **7c** with bulky molecular volumes show much improved PLQY of 1.13% and 1.77% (*vide* Table 3). It should be pointed out here that the measurement of absolute PLQYs in nitrogen is precluded by our experimental limitations, and therefore has to be carried out in air. As each complex studied here is found to show some emission quenching by oxygen, the QYs reported here should be lower than those measured in nitrogen atmosphere.

All these preliminary investigations on photophysical property suggest that **7a–7d** are attractive candidates for both oxygen sensor agents and emitting phosphors in PhOLEDs.

Electrochemical data

The electrochemical behaviors of these Ir(III) complexes are investigated by cyclic voltammetry in argon purged 5×10^{-4} mol L^{-1} CH_2Cl_2 solution with Fc/Fc^+ redox couple as an internal reference. The cyclic voltammograms of **(pbt)$_2$Ir(acac)**, **7c** and **7d** are shown in Fig. 6. During the anodic scan, each of these complexes exhibits a reversible one-electron oxidation wave in the range of 0.41~0.51 V, which is mainly attributed to the Ir(III/IV) metal center.[47] No reduction wave has been detected because of the limited range available in CH_2Cl_2. The HOMO energy levels of the compounds can be roughly estimated by comparison with the Fc/Fc^+ redox couple (whose energy level is 4.80 eV below vacuum),[36] and those of LUMO are deduced from the HOMO energies and optical bandgaps.[47]

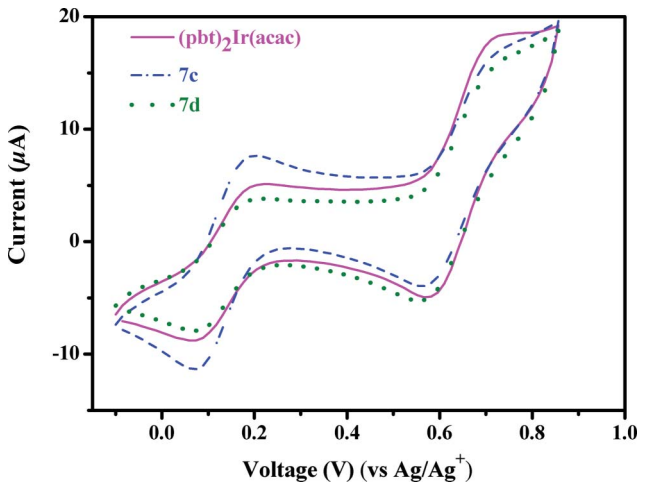

Fig. 6 Cyclic voltammograms of **(pbt)$_2$Ir(acac)**, **7c** and **7d**. The oxidation potentials are determined relative to Ag/Ag^+ in 5×10^{-4} mol L^{-1} CH_2Cl_2 solution, using ferrocene as internal reference.

The oxidation wave values of **7a–7c** are quite akin to that of **(pbt)$_2$Ir(acac)**, therefore the additional twisted phenyls would bring little influence to the HOMO of the complexes; yet **7d** bearing coplanarly bonded phenyl has an elevated HOMO of ~0.1 eV. On the other hand, all of the four target complexes show unexpected declined LUMOs of ~0.1 eV relative to **(pbt)$_2$Ir(acac)**, indicating that the *para*-substituented phenyls, either twisted or coplanar with the adjacent phenyl moieties of **pbt**, contributes similarly to the destabilization of LUMOs.

Theoretical calculation

DFT calculations are performed using Gaussian09 software to gain insights into the origin of the variable property induced by substitution. The optimized structures for the complexes along with the numbering of important atoms, main geometrical parameters calculated, and some experimental data of **7c** and **7d** derived from X-ray crystallography can be found in ESI.† The close similarity between calculated and experimental values reveals the reliability of our computation. Consistent with the experimental observations for **7c** and **7d**, all the biphenyl moieties in the optimized structures for **7a–7c** derived from calculation, show twisted geometry with dihedral angles of *ca.* 37°, while the fluorenyl segments in **7d** are calculated to be planar with torsion angles of *ca.* 0°.

The calculated HOMO energies, as shown in Table 4, accurately reproduce the experimental data. **(pbt)$_2$Ir(acac)** and **7a–7c** bearing additional distorted phenyl substituents possess analogous HOMO energy levels, while the introduction of a coplanar one (**7d**) would lead to elevated HOMO for 0.09 eV. Similar to those observed in Ir-ppy type complexes, the HOMOs of the objective Ir-**pbt** type complexes are dominated by Ir-d orbitals and π-orbitals of phenyl moieties directly connected to Ir atom

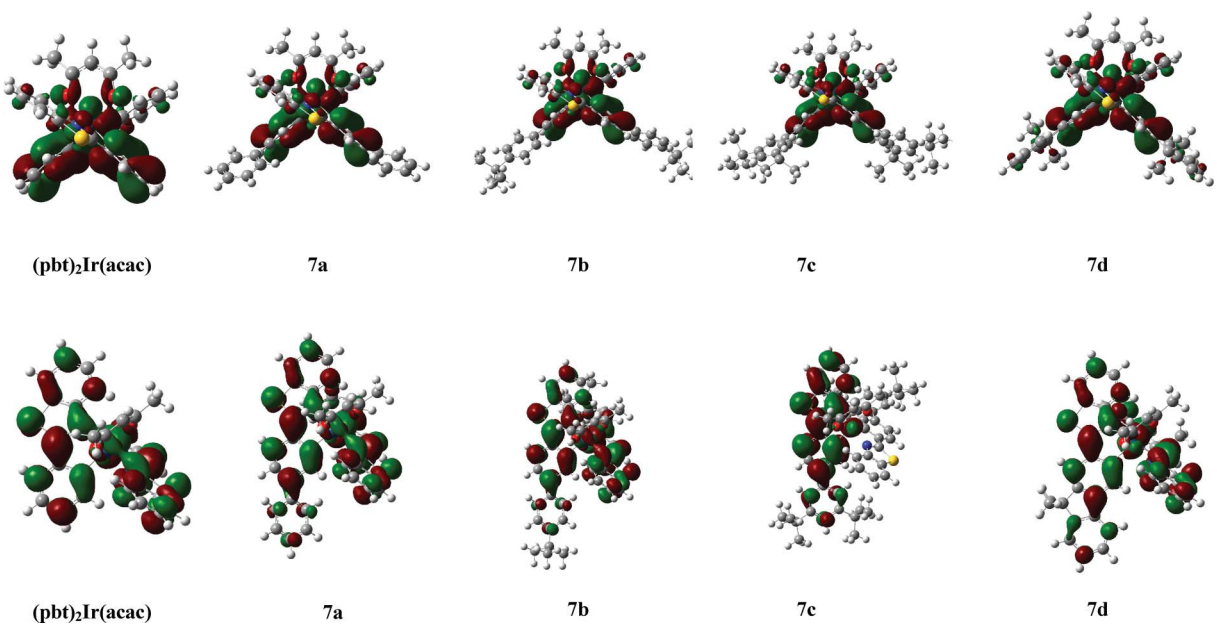

Fig. 7 Isodensity plots of the HOMO (top) and LUMO (bottom) for **(pbt)$_2$Ir(acac)** and **7a–7c**.

Table 5 Calculated singlet–singlet and singlet–triplet transitions (nm) for complexes **(pbt)$_2$Ir(acac)** and **7a–7d** using TDDFT method within the framework of the IEF-PCM Model in THF media, together with experimental values

Compound	**(pbt)$_2$Ir(acac)**	**7a**	**7b**	**7c**	**7d**
$S_0 \rightarrow S_1$[a]	453 (0.1174)	462 (0.1284)	462 (0.1354)	462 (0.1288)	477 (0.1454)
Character	MLCT/π–π*	MLCT/π–π*	MLCT/π–π*	MLCT/π–π*	MLCT/π–π*
Main configurations	H→L (100%)	H→L+1 (100%)	H→L+1 (100%)	H→L (100%)	H→L (59%), H→L+1 (41%)
	d(Ir)-π(C^N)→π*(C^N)	d(Ir)-π(C^N)→π*(C^N)	d(Ir)-π(C^N)→π*(C^N)	d(Ir)-π(C^N)→π*(C^N)	d(Ir)-π(C^N)→π*(C^N)
$S_0 \rightarrow S_n$[b]	n = 14	n = 10	n = 8	n = 8	n = 8
	306 (0.3209)	336 (0.1283)	364 (0.2511)	361 (0.5755)	369 (0.2215)
Character	MLCT/π–π*	π–π*	π–π*	π–π*	π–π*
Main configurations	H-5→L+1 (90%)	H-2→L (90%)	H-2→L (84%)	H-2→L+1 (85%)	H-3→L (77%)
	d(Ir)-π(C^N)→π*(C^N)	π(C^N + acac)→π*(C^N)	π(C^N + acac)→π*(C^N)	π(C^N + acac)→π*(C^N)	π(C^N)→π*(C^N)
	H-3→L+1 (8%)	H-3→L+1 (7%)	H-3→L+1 (9%)	H-3→L+1 (6%)	H-4→L (14%)
	d(Ir) + π(C^N)→π*(C^N)	d(Ir) + π(C^N)→π*(C^N)	d(Ir) + π(C^N)→π*(C^N)	d(Ir) + π(C^N)→π*(C^N)	d(Ir)-π(C^N)→π*(C^N)
					H-2→L+1 (6%)
					π(C^N + acac)→π*(C^N)
Emission exptl	557	578	578	577	600
$S_0 \rightarrow T_1$	512	532	534	530	562
Character	MLCT/π–π*	MLCT/π–π*	MLCT/π–π*	MLCT/π–π*	MLCT/π–π*
Main configurations	H→L (77%)	H→L (70%)	H→L (70%)	H→L (67%)	H→L (68%)
	d(Ir)-π(C^N)→π*(C^N)	d(Ir)-π(C^N)→π*(C^N)	d(Ir)-π(C^N)→π*(C^N)	d(Ir)-π(C^N)→π*(C^N)[a]	d(Ir)-π(C^N)→π*(C^N)
	H-1→L+1 (6%)	H-1→L+1 (12%)	H-1→L+1 (15%)	H-1→L (15%)	H-1→L+1 (21%)
	d(Ir)-π(acac)→π*(C^N)	d(Ir)-π(acac)→π*(C^N)	d(Ir)-π(acac)→π*(C^N)	d(Ir)-π(acac)→π*(C^N)	d(Ir)-π(acac)→π*(C^N)
	H-2→L+1 (13%)	H-2→L+1 (12%)	H-2→L+1 (10%)	H-2→L (11%)	H-2→L+1 (6%)
	π(C^N + acac)→π*(C^N)	π(C^N + acac)→π*(C^N)	π(C^N + acac)→π*(C^N)	π(C^N + acac)→π*(C^N)	π(C^N + acac)→π*(C^N)

[a] Data in parentheses are oscillate strength. [b] Denotes the strongest absorption band.

(orbital compositions are shown in Tables S2–S6 in ESI†). The contributions from Ir-d orbitals are calculated to be 49% for **(pbt)$_2$Ir(acac)**, 46~47% for **7a–7c**, and 42% for **7d**, and those from phenyl-π orbitals are nearly identical (33–34%). It can be seen obviously from Fig. 7 that the additional phenyl or *tert*-butyl substituents of **7a–7c** have little contribution (2–3%) to their HOMOs; yet in the case of **7d**, the coplanar phenyl and the methylene groups show visible donation to its HOMO (6%). Therefore, **(pbt)$_2$Ir(acac)** and **7a–7c** exhibit comparable features when considering the contribution from both center atom and substituents in their ground states, while **7d** displays higher HOMO energy.

The substituent effects on LUMOs, however, differs obviously from those on HOMOs, since different substituents on benzothiazole (*viz.*, biphenyl, *tert*-butyl modified biphenyl and fluorenyl) would result in similarly lowered LUMO energies of 0.07~0.11 eV relative to that of **(pbt)$_2$Ir(acac)**. According to the calculation results, all the LUMOs of the five complexes predominantly localize on the π* orbitals of benzothiazole segments [68% for **(pbt)$_2$Ir(acac)**, 60% for **7a–7c**, and 56% for **7d** (*vide* Tables S2–S6 in ESI†)]. Accompanied with the decreased donation composition of benzothiazole units, increased compensative contributions from the substituents (for **7a–7c**, *ca.* 8~9%, for **7d**, *ca.* 13%) can be found. It is noticeable that although the calculated LUMOs are significantly higher than those estimated from experiment (depicted in Table 4), the variation trends for both LUMO and HOMO–LUMO gap of the complexes show perfect reproduction between the calculation and experiment values. Thus compared with **(pbt)$_2$Ir(acac)**, the decreased band gaps for **7a–7c** can be merely assigned to their declined LUMOs, while **7d** having simultaneously destabilized HOMO and stabilized LUMO owns the lowest band gap.

To further investigate the nature of absorption and emission process involved in these phosphors, 20 low-lying singlet and triplet states of the complexes are calculated based on their optimized geometries of S_0 in THF solvent using TDDFT method, and the transition bands and characters of the relevant excited states are listed in Table 5. The calculated strongest absorption bands of the five compounds are comparable to their experimental values. Furthermore, our calculation reveals that the strongest absorption bands of **7a–7c** are dominated (84~90%) by the HOMO-2→LUMO/LUMO+1 transition with π(C^N + acac)→π*(C^N) configurations. That of **7d** shows a HOMO-3→LUMO predominated (77%) π(C^N)→π*(C^N) transition; yet **(pbt)$_2$Ir(acac)** is found to have its strongest absorption band dominated (90%) by the HOMO-5→LUMO+1 transition showing a mixed MLCT/π→π* feature (*vide* Table 5 and Tables S2–S6†). This may account for the different shapes of absorption curves observed experimentally between **(pbt)$_2$Ir(acac)** and **7a–7d** at 300–380 nm. The lowest singlet excited-states are calculated to locate at 453 nm for **(pbt)$_2$Ir(acac)**, 462 nm for **7a–7c**, and 477 nm for **7d**, which are analogous to their experimental values (447, 464, 463, 465 and 478 nm, successively), and all of them are assigned to HOMO→LUMO and HOMO→LUMO+1 transitions with MLCT/LC characters, where LUMO and LUMO+1 are calculated to be a degenerate couple with predominantly π* delocalized feature on benzothiazole moieties. Moreover, both the strongest transition bands and the lowest singlet excited-states of **7a–7d** are calculated to show bathochromic effect relative to **(pbt)$_2$Ir(acac)**, and **7d** has the lowest transition energy. All these computational results are consistent with the experimental facts.

The vertical excitation bands and the orbitals of the complexes involved in the dominant excitations for the lowest triplet states are depicted in Table 5. The T_1 states for all these complexes are similar in main configurations with only slightly different weight. The largest contribution of them (67%–77%) can be assigned to the HOMO–LUMO transitions, displaying MLCT/π→π* characters derived from d(Ir)-π(C^N + acac)→π*(C^N). The emission peaks calculated from T_1 states locate in 512, 532, 534, 530 and 562 nm for **(pbt)$_2$Ir(acac)** and **7a–7d**, successively. Despite the relatively large derivation from their actual λ_{PLmax} data, the calculated 18–22 nm red-shift for **7a–7c** and 50 nm for **7d** relative to **(pbt)$_2$Ir(acac)** are in accordance with the experimental facts (*ca.* 20–21 nm for **7a–7c**, and 43 nm for complex **7d**).

Conclusion

The substituent effects of four **(pbt)$_2$Ir(acac)**-type complexes on emission color and φ_{PL} have been investigated. By attaching an extra phenyl substituent to the *para*-site of phenyl in **pbt**, the emission color of the complexes could be fine-tuned to orange and red, and coplanar one is demonstrated to be more effective for achieving bathochromic shift of PL emission. The incorporation of *tert*-butyls with the chelates is proven to be an impactful way for the enhancement of PL efficiency. Both CV measurement and DFT calculation results reveal that the addition of a distorted phenyl substituent to phenyl segment of **pbt** ligands would lead to a declined LUMO rather than elevated HOMO; while the alteration of the twisted phenyl into a coplanar one would lead to both higher HOMO and lower LUMO. All these objective molecules show emission quenching by molecular oxygen in solution, and two of them even show efficient oxygen quenching in solid state. As all these complexes have appropriate PL quantum yields, emission colors and emission lifetime, they are prospective electrophosphors and oxygen sensing agents.

Acknowledgements

The authors acknowledge the financial support for this work by the National Natural Science Foundation of China (Projects 20872103, 50803040 and 20973115). We are grateful to the analytical and testing center of Sichuan University for providing NMR, X-ray single crystal analysis, UV-Vis and PL data for the intermediates and objective compounds.

References

1 (*a*) M. A. Baldo, D. F. O'Brien, Y. You, A. Shoustikov, S. Sibley, M. E. Thompson and S. R. Forrest, *Nature*, 1998, **395**, 151; (*b*) E. L. Williams, K. Haavisto, J. Li and G. E. Jabbour, *Adv. Mater.*, 2007, **19**, 197; (*c*) B. Tong, Q. Mei, S. Wang, Y. Fang, Y. Meng and B. Wang, *J. Mater. Chem.*, 2008, **18**, 1636.
2 (*a*) K. K.-W. Lo, C.-K. Chung, T. K.-M. Lee, L.-K. Lui, K. H.-K. Tsang and N. Zhu, *Inorg. Chem.*, 2003, **42**, 6886; (*b*) M. Yu, Q. Zhao, L. Shi, F. Li, Z. Zhou, H. Yang, T. Yi and C. Huang, *Chem. Commun.*, 2008, 2115.
3 (*a*) H. Chen, Q. Zhao, Y. Wu, F. Li, H. Yang, T. Yi and C. Huang, *Inorg. Chem.*, 2007, **46**, 11075; (*b*) J. S. Y. Lau, P. K. Lee, K. H. K. Tsang, C. H. C. Ng, Y. W. Lam, S. H. Cheng and K. K. W. Lo, *Inorg. Chem.*, 2009, **48**, 708.

4 (*a*) C. Adachi, M. A. Baldo, M. E. Thompson and S. R. Forrest, *J. Appl. Phys.*, 2001, **90**, 5048; (*b*) H. Sasabe, Y. J. Pu, K. Nakayama and J. Kido, *Chem. Commun.*, 2009, 6655; (*c*) Z. Jiang, Y. Chen, C. Yang, Y. Cao, Y. Tao, J. Qin and D. Ma, *Org. Lett.*, 2009, **11**, 1503.

5 (*a*) R. Meerheim, R. Nitsche and K. Leo, *Appl. Phys. Lett.*, 2008, **93**, 043310; (*b*) J. H. Jou, S. M. Shen, S. H. Chen, M. H. Wu, W. B. Wang, H. C. Wang, C. R. Lin, Y. C. Chou, P. H. Wu and J. J. Shyue, *Appl. Phys. Lett.*, 2010, **96**, 143306; (*c*) Y. Tao, Q. Wang, L. Ao, C. Zhong, J. Qin, C. Yang and D. Ma, *J. Mater. Chem.*, 2010, **20**, 1759.

6 F. M. Hwang, H. Y. Chen, P. S. Chen, C. S. Liu, Y. Chi, C. F. Shu, F. I. Wu, P. T. Chou, S. M. Peng and G. H. Lee, *Inorg. Chem.*, 2005, **44**, 1344.

7 (*a*) Y. T. Huang, T. H. Chuang, Y. L. Shu, Y. C. Kuo, P. L. Wu, C. H. Yang and I. W. Sun, *Organometallics*, 2005, **24**, 6230; (*b*) Y. Y. Lyu, J. Kwak, W. S. Jeon, Y. Byun, H. S. Lee, D. Kim, C. Lee and K. Char, *Adv. Funct. Mater.*, 2009, **19**, 420.

8 (*a*) Z. Liu, M. Guan, Z. Bian, D. Nie, Z. Gong, Z. Li and C. Huang, *Adv. Funct. Mater.*, 2006, **16**, 1441; (*b*) R. Meerheim, S. Scholz, S. Olthof, G. Schwartz, S. Rebastianeineke, K. Walzer and K. Leo, *J. Appl. Phys.*, 2008, **104**, 014510/1.

9 J. Qiao, L. Duan, L. Tang, L. He, L. Wang and Y. Qiu, *J. Mater. Chem.*, 2009, **19**, 6573.

10 (*a*) S. Lamansky, P. Djurovich, D. Murphy, F. Abdel-Razzaq, H. E. Lee, C. Adachi, P. E. Burrows, S. R. Forrest and M. E. Thompson, *J. Am. Chem. Soc.*, 2001, **123**, 4304; (*b*) M. L. Xu, G. Y. Wang, R. Zhou, Z. W. An, Q. Zhou and W. L. Li, *Inorg. Chim. Acta*, 2007, **360**, 3149.

11 (*a*) A. B. Tamayo, S. Garon, T. Sajoto, P. I. Djurovich, I. M. Tsyba, R. Bau and M. E. Thompson, *Inorg. Chem.*, 2005, **44**, 8723; (*b*) L. He, L. Duan, J. Qiao, D. Zhang, L. Wang and Y. Qiu, *Org. Electron.*, 2010, **11**, 1185; (*c*) C. F. Li, G. P. Yong and Y. Z. Li, *Inorg. Chem. Commun.*, 2010, **13**, 179.

12 W. C. Chang, A. T. Hu, J. P. Duan, D. K. Rayabarapu and C. H. Cheng, *J. Organomet. Chem.*, 2004, **689**, 4882.

13 (*a*) A. B. Tamayo, B. D. Alleyne, P. I. Djurovich, S. Lamansky, I. Tsyba, N. N. Ho, R. Bau and M. E. Thompson, *J. Am. Chem. Soc.*, 2003, **125**, 7377; (*b*) C. H. Yang, S. W. Li, Y. Chi, Y. M. Cheng, Y. S. Yeh, P. T. Chou, G. H. Lee, C. H. Wang and C. F. Su, *Inorg. Chem.*, 2005, **44**, 7770; (*c*) K. Dedeian, J. Shi, N. Shepherd, E. Forsythe and D. C. Morton, *Inorg. Chem.*, 2005, **44**, 4445; (*d*) S. Bettington, M. Tavasli, M. R. Bryce, A. Beeby, H. Al-Attar and A. P. Monkman, *Chem.–Eur. J.*, 2007, **13**, 1423.

14 (*a*) M. Tavasli, S. Bettington, M. R. Bryce, H. A. Al Attar, F. B. Dias, S. King and A. P. Monkman, *J. Mater. Chem.*, 2005, **15**, 4963; (*b*) C. H. Yang, C. H. Chen and I. W. Sun, *Polyhedron*, 2006, **25**, 2407.

15 (*a*) G. Zhou, C. L. Ho, W. Y. Wong, Q. Wang, D. Ma, L. Wang, Z. Lin, T. B. Marder and A. Beeby, *Adv. Funct. Mater.*, 2008, **18**, 499; (*b*) G. J. Zhou, Q. Wang, W. Y. Wong, D. Ma, L. Wang and Z. Lin, *J. Mater. Chem.*, 2009, **19**, 1872.

16 I. R. Laskar and T. M. Chen, *Chem. Mater.*, 2004, **16**, 111.

17 S. Lamansky, P. Djurovich, D. Murphy, F. Abdel-Razzaq, R. Kwong, I. Tsyba, M. Bortz, B. Mui, R. Bau and M. E. Thompson, *Inorg. Chem.*, 2001, **40**, 1704.

18 Y. You and S. Y. Park, *Dalton Trans.*, 2009, 1267.

19 (*a*) Md. K. Nazeeruddin, R. T. Wegh, Z. Zhou, C. Klein, Q. Wang, F. De Angelis, S. Fantacci and M. Grätzel, *Inorg. Chem.*, 2006, **45**, 9245; (*b*) H. J. Bolink, E. Coronado, R. D. Costa, N. Lardiés and E. Ortí, *Inorg. Chem.*, 2008, **47**, 9149.

20 S. Bernhard, J. A. Barron, P. L. Houston, H. D. Abruña, J. L. Ruglovksy, X. Gao and G. G. Malliaras, *J. Am. Chem. Soc.*, 2002, **124**, 13624.

21 X. Wei, J. Peng, J. Cheng, M. Xie, Z. Lu, C. Li and Y. Cao, *Adv. Funct. Mater.*, 2007, **17**, 3319.

22 T. Peng, H. Bi, Y. Liu, Y. Fan, H. Gao, Y. Wang and Z. Hou, *J. Mater. Chem.*, 2009, **19**, 8072.

23 (*a*) Rigaku/MSC (2005). *CrystalClear*, Rigaku/MSC Inc., The Woodlands, Texas, USA; (*b*) Oxford Diffraction (2009). *CrysAlisPro CCD and CrysAlisPro RED, including ABSPACK.* Oxford, Diffraction Ltd, Yarnton, England.

24 G. M. Sheldrick *SHELXL-,97, Program for Refinement of Crystal Structures*University of Göttingen, Göttingen, Germany, 1997.

25 (*a*) A. L. Spek, *J. Appl. Crystallogr.*, 2003, **36**, 7; (*b*) I. J. Bruno, J. C. Cole, P. R. Edgington, M. K. Kessler, C. F. Macrae, P. McCabe, J. Pearson and R. Taylor, *Acta Crystallogr., Sect. B: Struct. Sci.*, 2002, **B58**, 389.

26 (*a*) A. D. Becke, *J. Chem. Phys.*, 1993, **98**, 5648; (*b*) C. Lee, W. Yang and R. G. Parr, *Phys. Rev. B*, 1988, **37**, 785.

27 P. J. Hay, *J. Phys. Chem. A*, 2002, **106**, 1634.

28 C. Jarmorski, M. E. Casida and D. R. Salahub, *J. Chem. Phys.*, 1996, **104**, 5134.

29 E. Cancès, B. Mennucci and J. Tomasi, *J. Chem. Phys.*, 1997, **107**, 3032.

30 M. J. Frisch, G. W. Trucks, H. B. Schlegel, G. E. Scuseria, M. A. Robb, J. R. Cheeseman, G. Scalmani, V. Barone, B. Mennucci, G. A. Petersson, H. Nakatsuji, M. Caricato, X. Li, H. P. Hratchian, A. F. Izmaylov, J. Bloino, G. Zheng, J. L. Sonnenberg, M. Hada, M. Ehara, K. Toyota, R. Fukuda, J. Hasegawa, M. Ishida, T. Nakajima, Y. Honda, O. Kitao, H. Nakai, T. Vreven, J. J. A. Montgomery, J. E. Peralta, F. Ogliaro, M. Bearpark, J. J. Heyd, E. Brothers, K. N. Kudin, V. N. Staroverov, R. Kobayashi, J. Normand, K. Raghavachari, A. Rendell, J. C. Burant, S. S. Iyengar, J. Tomasi, M. Cossi, N. Rega, J. M. Millam, M. Klene, J. E. Knox, J. B. Cross, V. Bakken, C. Adamo, J. Jaramillo, R. Gomperts, R. E. Stratmann, O. Yazyev, A. J. Austin, R. Cammi, C. Pomelli, J. W. Ochterski, R. L. Martin, K. Morokuma, V. G. Zakrzewski, G. A. Voth, P. Salvado, J. J. Dannenberg, S. Dapprich, A. D. Daniels, O. Farkas, J. B. Foresman, J. V. Ortiz, J. Cioslowski, and D. J. Fox, *Gaussian 09*; A. 02 ed.; Gaussian, Inc.: Wallingford CT, 2009.

31 S. Murphy, X. Yang and G. B. Schuster, *J. Org. Chem.*, 1995, **60**, 2411.

32 X. Zhan, C. Risko, F. Amy, C. Chan, W. Zhao, S. Barlow, A. Kahn, J. L. Brédas and S. R. Marder, *J. Am. Chem. Soc.*, 2005, **127**, 9021.

33 F. Picard, T. Schulz and R. W. Hartmann, *Bioorg. Med. Chem.*, 2002, **10**, 437.

34 I. Mutule and E. Suna, *Tetrahedron*, 2005, **61**, 11168.

35 (*a*) F. O. Garces, K. A. King and R. J. Watts, *Inorg. Chem.*, 1988, **27**, 3464; (*b*) S. Sprouse, K. A. King, P. J. Spellane and R. J. Watts, *J. Am. Chem. Soc.*, 1984, **106**, 6647.

36 L. Chen, C. Yang, J. Qin, J. Gao and D. Ma, *Inorg. Chim. Acta*, 2006, **359**, 4207.

37 S. Takizawa, Y. Sasaki, M. Akhtaruzzaman, H. Echizen, J. Nishida, T. Iwata, S. Tokitoac and Y. Yamashita, *J. Mater. Chem.*, 2007, **17**, 841.

38 (*a*) K. A. McGee, D. J. Veltkamp, B. J. Marquardt and K. R. Mann, *J. Am. Chem. Soc.*, 2007, **129**, 15092; (*b*) K. A. McGee, B. J. Marquardt and K. R. Mann, *Inorg. Chem.*, 2008, **47**, 9143.

39 S. Jung, Y. Kang, H. S. Kim, Y. H. Kim, C. L. Lee, J. J. Kim, S. K. Lee and S. K. Kwon, *Eur. J. Inorg. Chem.*, 2004, **17**, 3415.

40 (*a*) A. Tsuboyama, H. Iwawaki, M. Furugori, T. Mukaide, J. Kamatani, S. Igawa, T. Moriyama, S. Miura, T. Takiguchi, S. Okada, M. Hoshino and K. Ueno, *J. Am. Chem. Soc.*, 2003, **125**, 12971; (*b*) J. P. Duan, P. P. Sun and C. H. Cheng, *Adv. Mater.*, 2003, **15**, 224.

41 (*a*) J. Van, Houten and R. J. Watts, *J. Am. Chem. Soc.*, 1975, **97**, 3843; (*b*) J. Van, Houten and R. J. Watts, *J. Am. Chem. Soc.*, 1976, **98**, 4853.

42 E. M. Kober, J. V. Caspar, R. S. Lumpkin and T. J. Meyer, *J. Phys. Chem.*, 1986, **90**, 3722.

43 (*a*) H. Z. Xie, M. W. Liu, O. Y. Wang, X. H. Zhang, C. S. Lee, L. S. Hung, S. T. Lee, P. F. Teng, H. L. Kwong, H. Zheng and C. M. Che, *Adv. Mater.*, 2001, **13**, 1245; (*b*) T. Qin, J. Ding, L. Wang, M. Baumgarten, G. Zhou and K. Müllen, *J. Am. Chem. Soc.*, 2009, **131**, 14329.

44 W. Holzer, A. Penzkofer and T. Tsuboi, *Chem. Phys.*, 2005, **308**, 93.

45 E. Vanderdonckt, B. Camerman, F. Hendrick, R. Herne and R. Vandeloise, *Bull. Soc. Chim. Belg.*, 1994, **103**, 207.

46 H. A. Bronstein, C. E. Finlayson, K. R. Kirov, R. H. Friend and C. K. Williams, *Organometallics*, 2008, **27**, 2980.

47 K. R. J. Thomas, M. Velusamy, J. T. Lin, C. H. Chien, Y. T. Tao, Y. S. Wen, Y. H. Hu and P. T. Chou, *Inorg. Chem.*, 2005, **44**, 5677.

